metals

MDPI

Article

Enhancing Mechanical Characteristics of 6061-T6 with 5083-H111 Aluminum Alloy Dissimilar Weldments: A New Pin Tool Design for Friction Stir Welding (FSW)

Wazir Hassan Khalafe [1,*], Ewe Lay Sheng [1], Mohd Rashdan Bin Isa [1] and Shazarel Bin Shamsudin [2]

[1] Department of Mechanical Engineering, Universiti Tenaga Nasional, Kajang 43000, Malaysia; laysheng@uniten.edu.my (E.L.S.); mrashdan@uniten.edu.my (M.R.B.I.)
[2] Department of Manufacturing Engineering, Universiti Tun Hussein Onn Malaysia, Parit Raja 86400, Malaysia; shazarel@uthm.edu.my
* Correspondence: pe20975@student.uniten.edu.my; Tel.: +60-11115-65060

Abstract: This research addresses the escalating need for lightweight materials, such as aluminum and magnesium alloys, in the aerospace and automotive sectors. The study explores friction stir welding (FSW), a cost-efficient process known for producing high-quality joints in these materials. The experiment involved the welding of dissimilar aluminum alloys (AA5086-H111 to AA6061-T6) using a novel pin tool design with welding parameters such as holding time, pin tool length, tool spindle speed, and linear speed fine-tuned through a design of experiment (DOE) approach. A comparative analysis of two tool designs revealed that the newly introduced design substantially improved mechanical properties, particularly tensile strengths, by 18.2% relative to its predecessor. It is noteworthy that FSW joint efficiency is 83% when using a normal tool design in comparison with 92.2% when using a new tool design at similar FSW parameters. The new tool achieved the parameter values leading to the maximum tensile strength of 317 MPa with 3 mm thickness (Th), 25 s holding time (Tt), 0.1 mm dimension (L), 1600 rpm spindle speed (SS), and 30 mm/min feed velocity (Fr). In comparison, the normal tool achieved a maximum UTS of 285 MPa, 5 mm Th, 25 s Tt, 0.3 mm L, 800 rpm SS, and 90 mm/min Fr. The new tool design, with longitudinal and circular grooves, improves heat input for plastic deformation and alloy mixing during welding. Subsequent analysis of the joint's microstructure and microhardness shows its similarity to the original alloys.

Keywords: aluminum alloy; friction stir welding; new tool design; microstructure; mechanical properties

Citation: Khalafe, W.H.; Sheng, E.L.; Bin Isa, M.R.; Shamsudin, S.B. Enhancing Mechanical Characteristics of 6061-T6 with 5083-H111 Aluminum Alloy Dissimilar Weldments: A New Pin Tool Design for Friction Stir Welding (FSW). *Metals* **2024**, *14*, 534. https://doi.org/10.3390/met14050534

Academic Editor: Yufeng Sun

Received: 25 March 2024
Revised: 28 April 2024
Accepted: 28 April 2024
Published: 30 April 2024

1. Introduction

Friction stir welding (FSW) was developed at the UK's Welding Institute in 1990, with additional funding from NASA in 1991 [1,2]. This technique revolutionized the welding of previously challenging materials like aircraft-grade 2000, 7000, and rail rolling stock's 6000 aluminum alloy series [3]. Notably, aluminum alloys 5083 and 6061, known for their mechanical strength and lightweight properties, became widely used in the aerospace, automotive, and maritime sectors [4]. Traditional methods of joining these alloys were flawed, prompting work by heating the base metal to a temperature below its recrystallization point, driving the need for alternatives. Aluminum alloys are occasionally subjected to heat treatment. Alloys' recrystallization temperatures can range from 340 °C to 400 °C. Care must be taken while applying the temperature and heating rate because they are unique to the alloy. Recrystallization reduces the metal's strength, increases its ductility, and lessens the density of displacements. According to [4,5], pinning grain boundary movement can cause a significant decline in the amount of recrystallized material at a slight decrease in hardening temperature. Stir welding (SW) emerged as an effective solution for welding aluminum and magnesium alloy [5]. It is a solid-state method, well suited

for low-melting alloys like AA6061 and AA5083. It primarily aims to achieve ultimate tensile strength (UTS) [6]. In one study, the UTS achieved was 194.3 MPa in a dissimilar FSW of AA5083 and AA6061-T6 compared to the base metals, indicating weaker tensile properties than the base metal [7]. Research also investigated welding techniques and tool design impacts, noting specific flaws in the weld [8]. The principle of FSW is simple: two metal plates are joined using a unique pin tool. The friction from the pin's motion softens the metals, effectively joining them [9]. In practice, different parameters can yield varied results. For instance, using specific tool designs and welding conditions, 5 mm thick AA6061 and AA5083 aluminum alloys achieved a UTS of 185.5 MPa [10]. Meanwhile, another set of conditions produced a joint with a UTS of 192.45 MPa [11]. Different tool geometries, when applied to 5 mm thick AA5083-H111 and AA6061-T6, resulted in varied UTS values, and [12] further explored FSW, using varied speeds and a specialized tool. Their research found an optimal UTS of 197 MPa under certain conditions [13]. Tools remain central in FSW, and while there is no standard design, researchers continually adapt to metal requirements such as eradication of tool tilt and control of softened work piece material [14]. Several papers highlighting the influence of processing parameters on joint properties, for example, refs. [15,16], reported parameters such as welding speed and tool rotational speed on joint characteristics, mechanical properties, and microstructure in lap joints and butts [17]. Reported microstructural features, mechanical, and thermal cycle properties for recrystallized grains. Tungsten carbide tools with 7% cobalt are standard for carbon steel welding (e.g., AISI 1018), whereas high-carbon steel tools are used for aluminum alloys. Specialized designs are employed in overlay welding and bobbin tool FSW. FSW lacks a fixed tool design, leading researchers to innovate for each metal's unique requirements. Miguel A. R. Pereira et al. [18] joined aluminum alloy AA6082-T6 (1 mm thick) and (6 mm thick) PA6 by friction stir spot welding (FSSW). The increase in plunge depth leads to an increase in mechanical strength up to the point where excessive penetration (0.5 mm) gives rise to rupture of the aluminum plate. M Ahmadi et al. [19] welded two 2 mm thick Al 6061 sheets, using three principal FSW parameters, namely, pin geometry, welding, and rotating speeds, each changing in three levels. By employing an L9 Taguchi orthogonal array, results have revealed that the highest fracture toughness belonged to the weld conducted using a square-shaped pin. P. Satish Kumar et al. [20] used friction stir welding to join 5 mm thick plates of AA5083 and AA6061 aluminum alloys in a butt-joint configuration. The tools employed were cylindrical, tapered, and square pins with threads, operated at speeds of 710, 900, and 1400 rpm and corresponding feed rates of 31, 40, and 60 mm/min, respectively. The optimal conditions achieved a maximum tensile strength of 191.62 MPa and a yield strength of 139.65 MPa with significant improvements in elongation, impact resistance, and hardness. Sanjeev Verma and his team [21] employed friction stir welding on 6 mm thick AA6061 and AA5083 aluminum alloys using various pin profiles (straight cylindrical, taper cylindrical, and square) at rotational speeds of 1200, 1575, and 1950 rpm, and feed rates of 30, 40, and 50 mm/min. They recorded a peak tensile strength of 141.33 MPa under these conditions. Saad Ahmed Khodir et al. [22] investigated the welding of 3 mm thick 2024-T3 and 7075-T6 aluminum alloys using an SKD61 steel tool with a 12 mm diameter shoulder and a 4.0 mm diameter threaded pin, achieving an ultimate tensile strength of 395 MPa. Microstructural examination revealed homogeneity in the stirred zone. In another study, [23], friction stir welding of 4 mm thick AA6082 and AA2024 alloys was explored. The tool, with a 3.8 mm pin length, was operated at 1600 rpm and 80 mm/min feed rate, focusing on fatigue resistance, which indicated a failure at 390,000 cycles at 100 MPa stress. K. Senthil Kumar and associates [7] analyzed the mechanical properties and microstructure of 6 mm thick dissimilar AA5083/AA6061 aluminum alloy joints welded with a taper-threaded pin at 1000 rpm and 25 mm/min. They noted an ultimate strength of 194.3 MPa and a joint efficiency of 61.5%, with varying hardness across different zones due to fine equiaxed recrystallized grains. In the research [24], a hybrid shoulder friction stir welding (HS-FSW) process was developed combining the advantages of rotational shoulder friction stir welding (RS-FSW) and nonrotational shoulder friction stir welding

(NRS-FSW). Both static and fatigue performance of the HS-FSW AleMgeSi alloy joints were examined and compared with those of the RS-FSW and NRS-FSW joints. The ultimate tensile strengths of the joints welded by HS-FSW were increased by 17.3 % and 6.7 %, compared with those of RS- and NRS-FSW, respectively. Research by Petr Homola et al. [25] introduced a tool made from metal matrix composite material coated with diamond-like carbon for friction stir spot welding. The tool, with a 16 mm diameter clamping ring, 7 mm shoulder, and 4 mm probe, operated at 1200 rpm and a plunge depth of 2.2 mm under a 13.5 kN force, showed promising results without leaving an exit hole. In the work [26], plates were prepared for an FSW joint from aluminum alloys (AA6061-T6 with AA2024-T3) at different feeding speeds (25, 30, 35, and 40) mm/min and fixed rotational speed of 1200 rpm. High-carbon steel was used in manufacturing of the tool, with dimensions of 20 mm shoulder diameter and a pin of 5 mm diameter and 4 mm length. The generated heat and plastic deformation resulting from the frictional process caused grain refinement in the stir zone, which led to an increase in hardness in the stir zone and decrease in the heat-affected zone (HAZ) for all investigated specimens. Xiangwei Li et al. [27] conducted fatigue tests on AA5083-H321 and AA6061-T6 aluminum alloy joints created through butt and lap friction stir welding. The results highlighted the lowest fatigue resistance correlating with the local stress distribution. Chand Basha Shaik and his team [28] enhanced the strength of AA5083 H111 and AA6061 T6 sheets welded by friction stir welding with the addition of SiC nanopowder. Optimized parameters included welding speed, rotational speed, and nanopowder volume, as determined by response surface methodology, which led to increased mechanical strength at optimal conditions. Miguel A. R. Pereira et al. [29] study potential of the friction stir welding (FSW) and its variants to join fiber-reinforced thermoplastic polymer. The rotational speed and the welding speed have great influence on heat generation, mixture quality, and fiber fragmentation degree. Threaded or grooved conical pins achieved better results than other geometries. This research is focused on enhancing the mechanical properties of welded materials through innovations in FSW tool pin designs. These custom tool pin designs are tailored to match the precise requirements of different materials, resulting in better joint quality, fewer defects, and reduced stress during welding. This drive for efficiency, cost effectiveness, and eco-friendliness or environmental benefits (e.g., ensuring the safety of the workers; having no radiation, toxic emissions, or producing detrimental fumes) [30] is particularly valuable in FSW's wide-ranging applications, spanning from aerospace to manufacturing, as it contributes to lowering production costs. From the summarized research, it is evident that the highest recorded tensile strength in friction stir welding of AA6061 with AA5083 is 194.3 MPa, while AA2024-T3 with AA7075-T6 reached a maximum of 395 MPa. Tool design plays a crucial role in influencing the mechanical properties, fatigue resistance, and microstructural characteristics of the welded joints. Optimal conditions lead to a microstructure characterized by fine and equiaxed grains, contributing to homogeneity in the stirred zone (SZ). S. Jayaprakash et al. [31] welded two aluminum alloys (AA5083 and AA7068) by using a cylindrical taper tool. The minimum and maximum microhardness were obtained as 42 HV and 75 HV, respectively. The implementation of a triangular tool provided minimum and maximum microhardness of 48 HV and 86 HV, respectively, while the application of a straight cylindrical tool provided minimum and maximum microhardness of 46 HV and 82 HV, respectively. The triangular tool offered the maximum tensile strength and microhardness from this investigation. The hardness value and the ultimate tensile strength were increased in the welding zone, which proves that the effects of tool profiles are efficiently utilized. FSW simply modified the grain structure and also improved the strength of the joints for any type of alloying elements. The experimental study by Bekir Çevik et al. [32] investigated the effect of stirring tool materials on microstructure, mechanical properties, and residual stress of joints in samples of 7075-T651. The weld zone consisted of four zones: the base material zone, the heat-affected zone (HAZ), the TMAZ, and the weld metal zone showed different macrostructural properties. Our innovative pin tool design is crucial in influencing the mechanical and microstructural

characteristics of friction-stir-welded joints between 6061-T6 and 5083-H111 aluminum alloys. By optimizing heat generation, material flow, and mixing during the welding process, the design ensures enhanced surface contact and utilizes specific geometrical features for even heat distribution. This results in a uniformly mixed stirred zone with fine, equiaxed grains, significantly improving the mechanical strength and fatigue resistance of the weld. This critical design element is key to achieving superior quality in the weldments. Differences in hardness within the welds are notable, with lower values typically observed in less stirred areas and higher values in the intensely welded nugget. Friction-generated heat and plastic deformation promote grain refinement in the stir zone, enhancing hardness there while reducing it in the heat-affected zone (HAZ). Welds generally show reduced fatigue resistance, closely associated with local stress distribution. The primary objective of this study is to develop and evaluate a novel pin tool design for friction stir welding (FSW) that enhances the mechanical characteristics of dissimilar weldments between 6061-T6 and 5083-H111 aluminum alloys. By focusing on the optimization of tool geometry, our research aims to overcome the prevalent limitations in welding dissimilar aluminum alloys, such as reduced strength and irregular material flow (the uneven distribution and movement of material around the tool's pin and shoulder as it travels along the weld line), which have not been comprehensively addressed in existing studies. This advancement holds the potential to significantly improve the reliability and performance of welded structures in industries where aluminum alloys are pivotal, thereby offering a valuable resource for engineers and scientists seeking to push the boundaries of current welding technology. This study aims to create and assess a new pin tool design for friction stir welding (FSW) to improve the welding of different aluminum alloys, specifically 6061-T6 and 5083-H111. Our focus is on refining the tool's shape to fix common welding issues like weaker bonds and uneven material flow. By doing so, we hope to enhance the durability and efficiency of welded aluminum structures, providing a significant contribution to engineering and materials science fields.

2. Methods and Protocols

2.1. Experiment Procedure

In this study, the optimality criterion for selecting the best combination of welding parameters was based on a multi-faceted evaluation aimed at maximizing weld quality and efficiency. The criteria included maximizing mechanical strength and fatigue resistance, ensuring a fine, equiaxed microstructure in the stirred zone, minimizing process defects and tool wear, and achieving consistency and reproducibility across welds. These parameters were systematically optimized using factorial experiments and response surface methodology to identify settings that consistently produced superior outcomes across these key performance indicators. Different AA6061-T6 and AA5083-H111 alloys for plates have been used in the stir friction welding method. For aluminum alloys of AA6061-T6 and AA5083-H111, chemical and mechanical properties are shown in Tables 1 and 2. AA5083 is non-heat-treatable. AA6061 is treatable and accessible in different thermally treated attitude conditions. In data analysis, symbols are used to represent each parameter, as illustrated in Table 3. This Table plays a crucial role in elucidating the variables within the study and facilitating the understanding of how these parameters interact with one another. These parameters (Table 3) were selected based on the following factors validated and suggested by various studies in the literature: (i) higher thickness affects microstructure and hardness [33]; (ii) holding time is applied to optimize the bond diffusion between aluminum alloys [34]; (iii) pin length has an effect on welding tool microstructural changes [35,36]; (iv) spindle speed can significantly affect the generated heat input and its morphology [37]; and (v) the feed rate constant has an effect on dynamically recrystallized grains [38]. Ronald A. Fisher developed the idea of design of experiment (DOE) in 1920 by suggesting a systematic method to gather as much data as possible from experimental trials [39,40]. DOE was well received by researchers worldwide, since it significantly reduces the amount of time, cost, and labor required by eliminating pointless tests and observations through the use

of a proper DOE technique. In addition, the system's primary parameters, their relationships, and their contributions to the system's outcome can be thoroughly recognized and promptly recorded. We utilize a DOE method to evaluate the impact of five crucial FSW parameters (Table 3). The aluminum alloys AA6061 and AA5083 were chosen for the DOE because of their wide range of disposition condition-dependent mechanical and corrosion properties and weldability [41]. The experiment began with the preparation of the required raw materials, namely, aluminum alloys AA6061 and AA5083, with thickness variations of 3 mm, 4 mm, and 5 mm, employing a simplified work procedure. To attain the desired tensile strength in the welds, precision cutting was executed to create dimensions of 60 mm by 80 mm for a total of 19 sets, each consisting of 2 pieces, as shown in Table 4. Laser cutting machines were utilized for this purpose. Following material preparation, custom tool designs, represented in Figure 1a,b, were meticulously crafted to meet the research's specific requirements. The welding process employed the FSW technique, integrated into the DOE detailed in Table 4. The same DOE parameters were applied in two instances, one with the normal tool design and the other with the new tool design. To assess tensile strength, samples were cut according to ASTM Designation: E8/E8M 15a standards, using a CNC water jet for precise cutting. Ultimately, the samples underwent a tensile strength test to evaluate their mechanical properties. A detailed analysis of the microhardness and microstructure of the samples that exhibited the highest tensile strength using the new tool design was also conducted. The newly designed tool, as depicted in Figure 1a and Table 5, assumed a pivotal role in the FSW process. Its significance lay in its ability to furnish the necessary heat for efficient plastic deformation and promote the amalgamation of the alloys intended for welding. Through the application of a pertinent equation accounting for the thickness of the alloy being welded, the length of the tool pin, and the diameter of the shoulder tool, the optimal welding depth was accurately determined [42,43]. This was achieved by incorporating longitudinal and circular grooves.

Table 1. Chemical composition of the aluminum alloy standard (ISO AlMg1SiCu; Aluminum 6061-T6) and (Spec:BSEN573-3:20) [11].

Element	Mg	Mn	Zn	Fe	Cu	Si	Cr	Al
AA6061-T6	0.84	0.01	0.06	0.40	0.24	0.24	0.18	bal
AA5083-H111	0.01	0.27	5.1	0.13	6.7	0.01	1.2	bal

Table 2. Mechanical properties of aluminum alloys (ASTM B557M-02a) [11].

Element	Yield Stress (MPa)	Tensile Strength (MPa)	Elongation %
AA6061-T6	306	342	17
AA5083-H111	387	471	20

Table 3. Design of the process parameters.

Factor Symbol	Parameter	Level		
		Low (−1)	Center (0)	High (+1)
Th	Thickness (mm)	3	4	5
Tt	Holding time (s)	15	20	25
L	Length (mm)	0.1	0.2	0.3
SS	Spindle Speed (rpm)	800	1200	1600
Fr	Feed Rate (mm/min)	30	60	90

Table 4. Experimental design using half-factorial design.

Run Order	Input Parameters (Factors)				
	Th	**Tt**	**L**	**SS**	**Fr**
1	3	25	0.3	1600	90
2	3	15	0.3	800	90
3	5	25	0.1	1600	90
4	4	20	0.2	1200	60
5	3	25	0.1	1600	30
6	5	15	0.3	1600	90
7	3	25	0.1	800	90
8	5	25	0.3	1600	30
9	4	20	0.2	1200	60
10	3	15	0.1	1600	90
11	4	20	0.2	1200	60
12	5	15	0.1	1600	30
13	3	15	0.1	800	30
14	3	15	0.3	1600	30
15	3	25	0.3	800	30
16	5	25	0.3	800	90
17	5	15	0.3	800	30
18	5	25	0.1	800	30
19	5	15	0.1	800	90

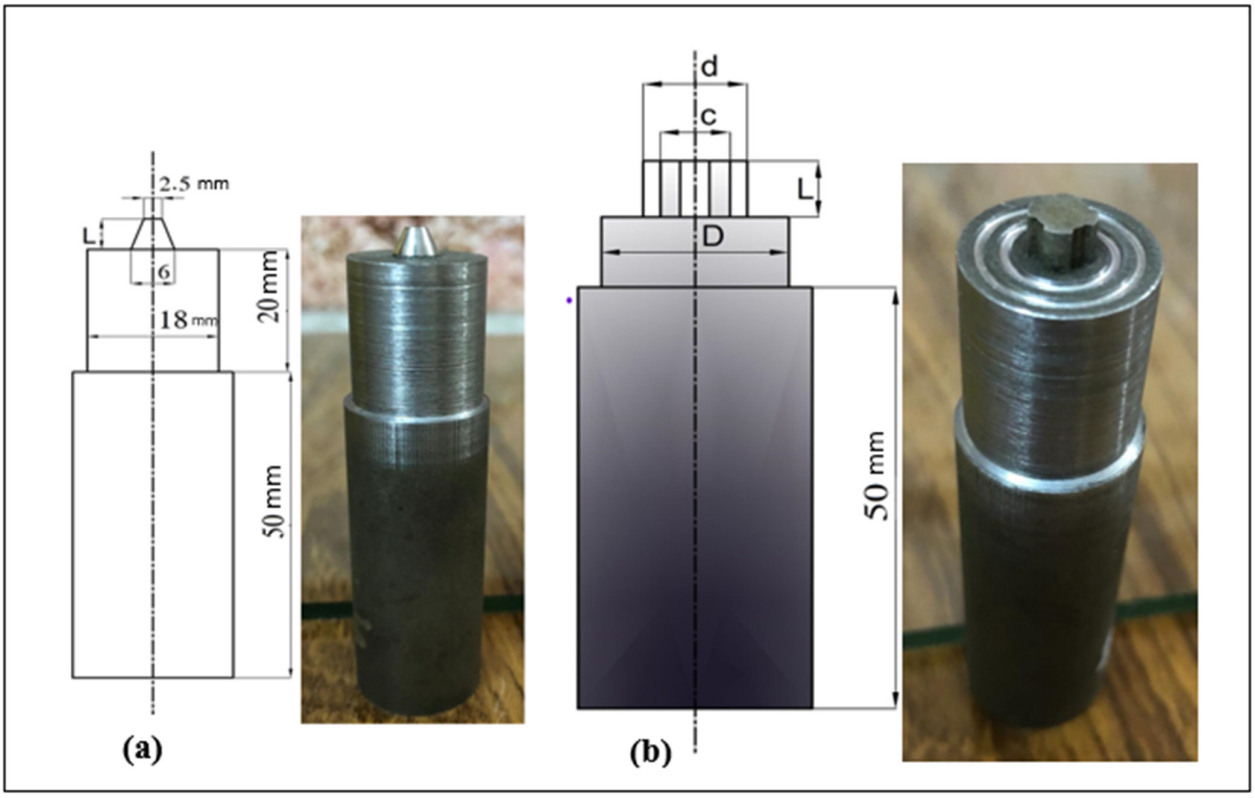

Figure 1. (**a**) Normal tool design (L = length of pin tool (less than the thickness of material to be welded (0.1, 0.2, 0.3 mm). (**b**) New tool design.

Table 5. New tool parameters.

	Dimension	Thickness
L	Length of tool pin (mm)	*d*—(0.1, 0.2, 0.3) mm, less than the material thickness for FSW welding
d	Diameter of tool pin (mm)	material thickness to be welded
C	*d*—1 mm, 1 mm, Depth digging groove × 2	Depth digging in surface of shoulder = 0.5 mm
D	Diameter of shoulder (mm)	(*d**3) + 2 mm [5]
	Pin profile: Cylindrical flat Tilt angle (1.6°)	

2.1.1. Design of Experiment

A reliable method for testing a hypothesis is the "DOE" approach. In this study, a half-factorial design with 2 replicates and 3 center points was chosen to execute the experiment, with a focus on factors such as material thickness, tool rotational speed (N), holding time, length of tool pin, and feed rate. The optimization of these parameters was considered through a range of settings, such as thickness of material (3 to 5 mm), holding time (15 to 25 s), length of tool pin (0.1 to 0.3 mm), rotational speed (800 to 1600 rpm), and feed rate (30 to 90 mm/min), as shown in Table 3. A 25-run strategy with a half-factorial design, including 2 repeats and 3 central points, was employed in this research. Table 4 shows the specific layout of the experimental procedures. The ultimate UTS of the joined material was measured. The response surface method (RSM) was used to examine the effects of different parameters, understand their interplay, and improve the outcome.

2.1.2. Testing Procedure

The mechanical characteristics of welded connections were determined in this work using the Charpy V-notch, tensile, and three-point bending tests. The tensile tests were conducted using pre-prepared samples that met the specifications of ISO 6892-1:2016. The tests were conducted at a crosshead speed on a sample with a 100 mm parallel length of 1 mm/min at a rate of 1 percent per minute using a Shimadzu AGX™-V2 testing machine (Kyoto, Japan). Three-point bending test samples were developed in compliance with EN ISO 5173:2023. The Charpy V-notch impact tests were conducted in compliance with ASTM E 2363:2023. Every sample underwent three sets of tests, and the average results were assessed. Vickers microhardness tests under 50 gf for 10 s were performed along the centerlines of the side surface of the welded samples in compliance with BS EN 1043-2:1997. Polished surfaces were etched using Keller solutions for microstructure analysis.

3. Results and Discussion

In this section, the mechanical properties of the welding method, with a specific focus on tensile strength, were examined. The effectiveness of the normal tool design was compared with that of the newly developed design, highlighting the clear advantages of the latter. Furthermore, an analysis of the microstructure to evaluate tensile strength when using the new tool design was conducted. D. Rahmatabadi et al. [44] studied, for the first time, the elastic and plastic parameters such as the elastic modulus, Poisson ratio, strength coefficient, strain hardening exponent, anisotropy coefficient, and yield stress of ARBed specimens which were extracted in the different ARB passes. The ultrafine-grained Al 1050 produced by the ARB procedure repeated to seven passes with 50% thickness. The analysis includes an assessment of microstructure to evaluate tensile strength with the new tool design (see Sections 3.1 and 3.2), as well as an examination of microhardness (see Section 3.3). These efforts aim to provide a deeper understanding of the material's mechanical behavior.

3.1. Mechanical Properties

3.1.1. With Normal Tool Design

In order to test the tensile strength using normal tool design, a total of 19 samples were used. Table 6 displays the achievement of the maximum UTS registration at 285 MPa. This was observed under specific settings: thickness (Th) measuring 5 mm, holding time (Tt) lasting 25 s, a dimension (L) of 0.3 mm, a rotational speed (SS) of 800 rpm, and a feed velocity (Fr) marked at 90. To facilitate a direct comparison, the tensile strength data obtained from the new tool design with data acquired using the conventional tool design have been contrasted. This provides a complete perspective on the tensile strength results produced by both tools. A linear-elastic behavior is expected from the sample, assuming that the machine operates without internal hysteresis. This is because the peak stress induced by this load is approximately 55.2 MPa, which remains below the yield stress threshold for various aluminum alloys. It may be inferred that the energy dissipation observed from the response of the joint is entirely attributable to friction occurrences inside the normal tool design because a linear load displacement was obtained throughout the experiment. This is because the energy dissipation of the loads increases with an increase in stress induction.

Table 6. Tensile strength results obtained using normal tool design.

Run Order	Input Parameters (Factors)					Response	
	Th	Tt	L	SS	Fr	Average Measured Value (TS)	% Error
1	3	25	0.3	1600	90	282	0.89
2	3	15	0.3	800	90	209	0.67
3	5	25	0.1	1600	90	211	0.80
4	4	20	0.2	1200	60	209	0.72
5	3	25	0.1	1600	30	282	0.57
6	5	15	0.3	1600	90	146	0.66
7	3	25	0.1	800	90	282	0.88
8	5	25	0.3	1600	30	227	0.68
9	4	20	0.2	1200	60	195	0.65
10	3	15	0.1	1600	90	155	0.78
11	4	20	0.2	1200	60	209	0.90
12	5	15	0.1	1600	30	155	1.23
13	3	15	0.1	800	30	146	0.94
14	3	15	0.3	1600	30	195	1.36
15	3	25	0.3	800	30	227	0.89
16	5	25	0.3	800	90	285	0.96
17	5	15	0.3	800	30	146	1.15
18	5	25	0.1	800	30	237	0.98
19	5	15	0.1	800	90	164	0.79

A settling cycle was applied before the tensile test. An applied cycle load is placed on the material during the test. A sinusoidal waveform is usually used to describe how the load differs between minimum and maximum values. The number of load cycles are sustain before failing in the tensile test.

Main Effect Plot for Tensile Strength (TS) (Normal Tool Design)

The optimal parameter settings, which were determined through RSM analysis, are presented in Tables 3 and 6 and display the tensile strength data obtained using the normal tool design. The DOE-recommended optimal parameters can result in achieving a maximum tensile strength of 296.57 MPa, with a normal tool design. Figure 2 illustrates the main effect plots, clearly demonstrating the relationship between the holding time (Tt} factor and the tensile strength (TS). It is evident that the TS decreases linearly as the thickness of the aluminum sheet increases, where the factors of tool pin length and feed rate show a positive impact on the TS response. Moreover, it is worth noting that lower

spindle speeds have a more favorable influence compared to higher speeds. The observed phenomena may be due to the decrease in tensile strength and increase in thickness of the aluminum sheet. This increased the holding time that allows dislocation, redisposition, and recovery of the material. However, the decrease in tensile strength with decreasing rotation speed may be due to the stir zone's hardness. A decrease in tensile strength is hypothesized to occur when the rotation speed is low because of some vacuums in the material flow [45]. The positive effect of tool pin length and feed rate on tensile strength is attributed to improved stirring, mixing, and grain refinement, leading to increased strength. Lower spindle speeds have a more favorable influence on tensile strength by minimizing heat generation, reducing grain growth, and promoting better material flow and grain structure.

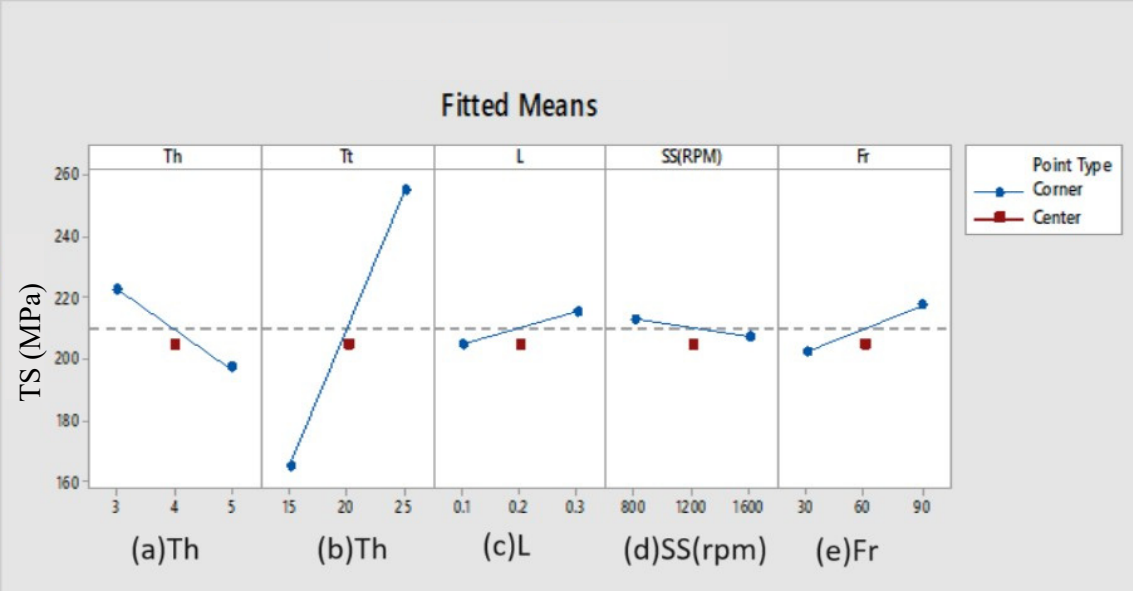

Figure 2. Main effect plot (TS). Note: thickness (Th), holding time (Tt), dimension (L), rotational speed (SS), and feed velocity (Fr).

3.1.2. With New Tool Design

In order to test the tensile strength using the new tool design, a total of 19 samples were used. The data collected through the testing process were compiled, and the outcomes are presented in Table 7. A central focus of this study is the utilization of FSW. Notably, tensile strength test results for samples welded using this new tool surpass those of the normal tool. This observation shows a substantial enhancement in mechanical properties, particularly tensile strength, and the optimization of the welding process achieved through the application of this new tool. The welding process, where materials are joined together, benefits significantly from this tool as it generates the requisite heat for inducing plastic deformation until the welding task is successfully completed. This improved performance can be primarily attributed to the longitudinal and circular dimensions, as well as the strategically integrated grooves within the design of the new tool.

Main Effect Plot for Tensile Strength (TS) (New Tool Design)

Figure 3 reveals the main effect plots, which provide valuable insights into the influence of various parameters on TS. Notably, the parameter values leading to the maximum tensile strength of 319.87 MPa are achieved with Th (5 mm), Tt (25 s), L (0.1 (97.5%) mm), SS (1600), and Fr (30 mm/min), the optimization plot for TS. In the main effect plot for TS, it is evident that TS exhibits a linear dependency on the holding time (Tt) factor, with a decreasing trend as the thickness of the aluminum sheet increases. Conversely, the lengths of the tool pin (L) and feed rate (Fr) factors positively impact the TS response. Furthermore, lower spindle speed (SS) yields a more favorable influence on TS compared to higher speeds.

Table 7. Tensile strength results obtained using new tool design.

No.	Input Parameters (Factors)							Response Average Measured Value (TS) MPa
	Thickness (mm)	Time Holding (Second)	Length (mm)	Rotation Tool Speed (rpm)	Linear Tool Speed (mm/min)	Yield Stress (MPa)	Elongation %	TS (MPa) Used New Design Tool
1	3	25	0.3	1600	90	255	0.512	285
2	3	15	0.3	800	90	240	8.335	280
3	5	25	0.1	1600	90	210	7.82	250
4	4	20	0.2	1200	60	210	0.817	245
5	3	25	0.1	1600	30	300	2.249	317
6	5	15	0.3	1600	90	195	0.92	197
7	3	25	0.1	800	90	270	1.14	290
8	5	25	0.3	1600	30	210	0.861	270
9	4	20	0.2	1200	60	230	0.531	240
10	3	15	0.1	1600	90	134	0.561	205
11	4	20	0.2	1200	60	140	0.878	245
12	5	15	0.1	1600	30	168	0.555	215
13	3	15	0.1	800	30	140	0.262	153
14	3	15	0.3	1600	30	142	0.923	220
15	3	25	0.3	800	30	215	8.65	250
16	5	25	0.3	800	90	230	1.07	285
17	5	15	0.3	800	30	194	1.037	196
18	5	25	0.1	800	30	270	9.301	278
19	5	15	0.1	800	90	66	0.703	190

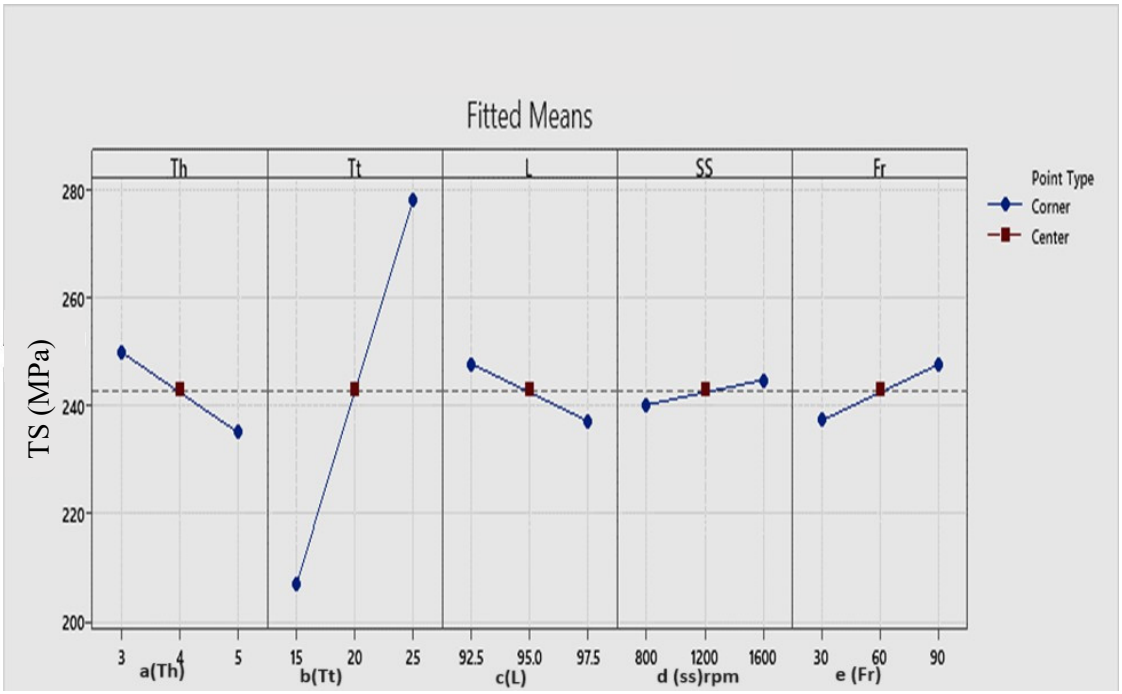

Figure 3. Main effect plot (tensile strength, TS) (new tool design). Note: thickness (Th), holding time (Tt), dimension (L), rotational speed (SS), and feed velocity (Fr).

Comparison of Tensile Strength between the New Tool Design and the Normal Tool Design in FSW

Table 8 provides an overview of the tensile strength development in each sample with identical FSW parameters while comparing the use of a new design tool to a conventional tool. A significant observation is that using the new design tool in FSW results in an 18.2% enhancement in tensile strength development compared to the normal tool. This suggests

that the updated tool design aids in achieving a better merge of the aluminum alloys, AA6061 and AA5083, leading to a more consistent plastic deformation with reduced flaws.

Table 8. The percentage variance in tensile strength between the new tool design and the normal tool design in FSW.

No.	TS (MPa) Normal Design Tool	TS (MPa) New Design Tool	Improvement (%)	Young's Modulus (GPa)
1	282	285	1.1	183
2	209	280	33.9	179
3	211	250	18.5	180
4	209	245	17.2	188
5	282	317	12.4	191
6	146	197	34.9	101
7	282	290	2.8	180
8	227	270	18.9	182
9	195	240	23	178
10	155	205	32.4	118
11	209	245	17.2	144
12	155	215	38.7	107
13	146	153	4.8	100
14	195	220	12.8	123
15	227	250	10.1	179
16	285	285	0	188
17	146	196	34.2	112
18	237	278	17.2	171
19	164	190	15.9	113

To further explore the effect, the results from the tensile tests were incorporated into our experimental design system for an in-depth review. The connection between the peak tensile strength reached in FSW (Max·TS·FSW) and the tensile strength inherent to the base alloys (TS of base alloys) was examined. Through this review, the FSW joint effectiveness ($\text{Efficiency}_{\text{FSW}}$) was calculated using the following equation (Equation (1)):

$$\text{Efficiency}_{\text{FSW}} = \frac{\text{Max·TS·FSW}}{\text{TS of Al 6061}} \times 100\% \quad (1)$$

where TS for base Al 6061 = 342 MPa [11].

With the normal tool design, the FSW joint efficiency was determined to be 83%, signifying that 83% of the base alloy's tensile strength remained in the joint. In contrast, the new tool design demonstrated a significantly higher FSW joint efficiency of 92.2%, highlighting its superior performance and effectiveness in creating stronger and more efficient welded joints.

3.2. Microstructural Analysis

Samples designated for microstructural analysis were carefully selected from FSW samples subjected to testing with the new tool design. These selected samples, labeled as 1, 2, 5, 7, 8, and 18 (Figure 4), displayed corresponding tensile strengths of 285, 280, 317, 290, 270, and 278 MPa, respectively. It is worth noting that all of these samples exhibited a high degree of homogeneity, rendering them well suited for welding dissimilar aluminum alloys, namely, AA6061 and AA5083.

Microstructural analysis showed that there was a strong link between tensile strength values. Upon careful examination of the scanning electron microscope (SEM) image presented in Figure 5, Samples 1, 2, 5, 7, 8, and 18 exhibit no observable cracking. This highlights the influence of welding conditions and tool design on the structural integrity of the welded joints. It highlights the importance of selecting appropriate parameters and tool designs to mitigate the risk of cracking and ensure the robustness of the resulting welds.

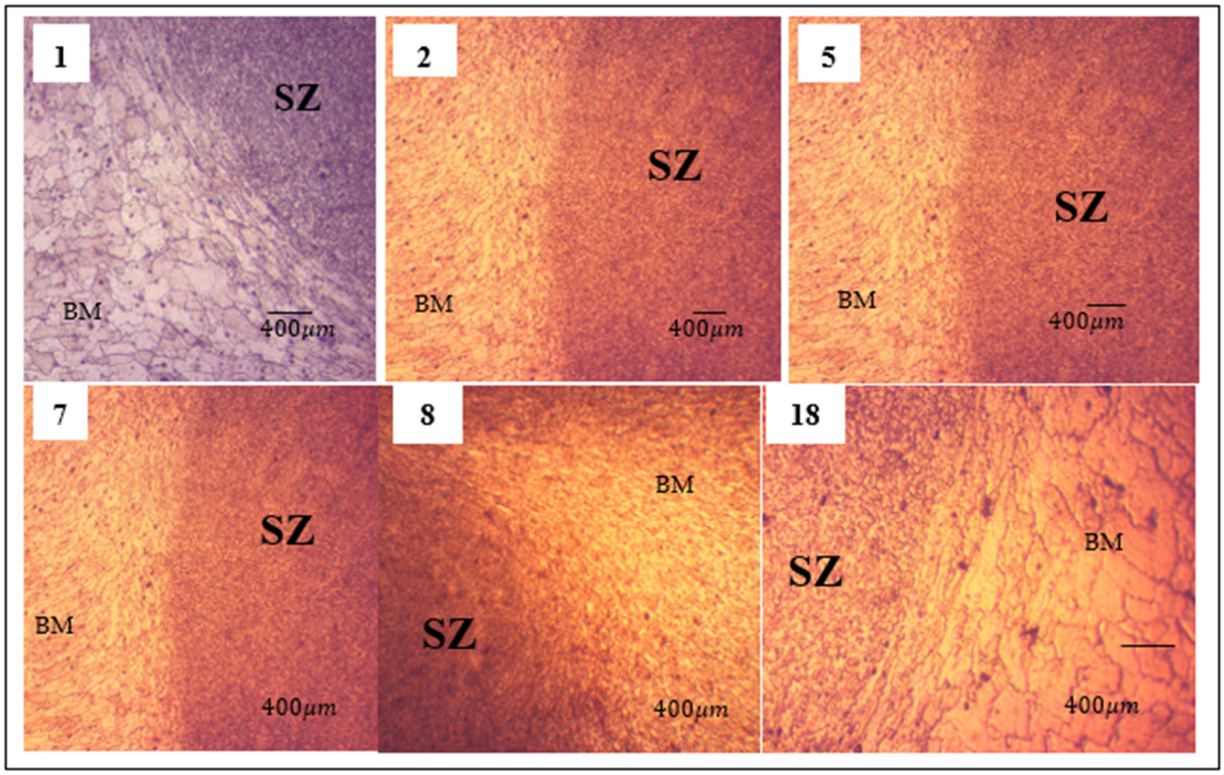

Figure 4. Microstructure of the optimum TS of FSW for the new tool design.

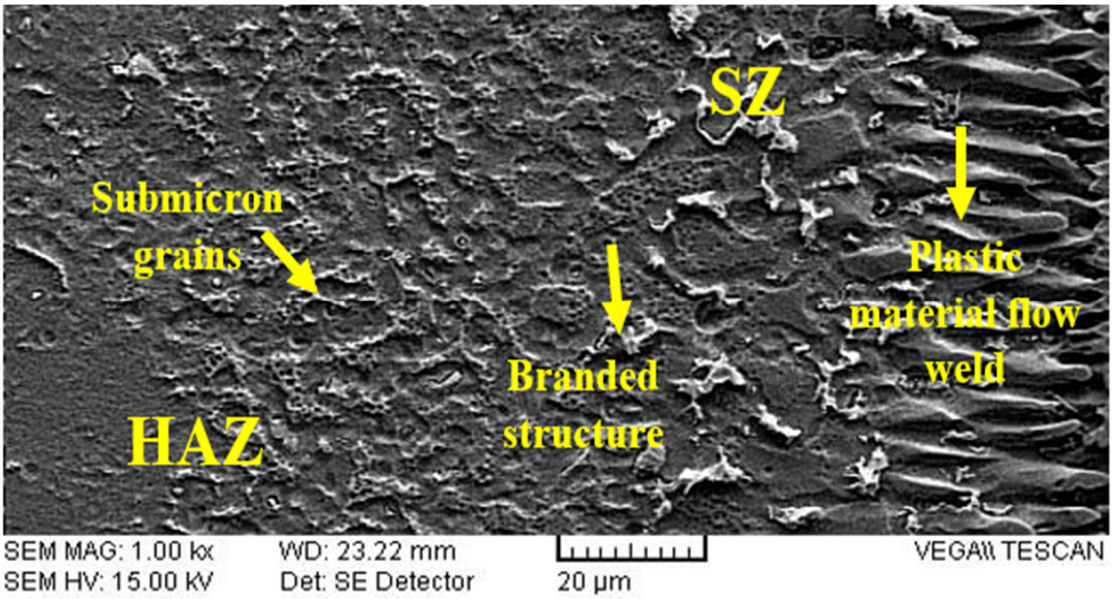

Figure 5. SEM at center of the weld [46]. Note: stir zone (SZ), heat-affected zone (HAZ).

1. Sample 1: TS 285 MPa (Th 3 mm, Tt 25 s, L 0.3 mm, SS 1600 rpm, Fr 90 mm/min)
2. Sample 2: TS 280 MPa (Th 3 mm, Tt 15 s, L 0.3 mm, SS 800 rpm, Fr 90 mm/min)
3. Sample 5: TS 317 MPa (Th 3 mm, Tt 25 s, L 0.1 mm, SS 1600 rpm, Fr 30 mm/min)
4. Sample 7: TS 290 MPa (Th 3 mm, Tt 25 s. L 0.1 mm, SS 800 rpm, Fr 90 mm/min)
5. Sample 8: TS 270 MPa (Th 5 mm, Tt 25 s, L 0.3 mm, SS 1600 rpm, Fr 30 mm/min)
6. Sample 18: TS 278 MPa (Th 5 mm, Tt 25 s, L 0.1 mm, SS 800 rpm, Fr 30 mm/min)

Previous studies by [46] on FSW of AA5083 with AA6061, utilizing various tool designs like taper tool pins, threaded tool pins, and cylindrical tool pins, revealed distinct

microstructures (Figure 4) characterized by two regions: the stir zone (SZ) and the heat-affected zone (HAZ). Furthermore, ref. [20] conducted FSW of AA6061 with AA5083, employing a threaded tool pin profile, and achieved a tensile strength of 191.62 MPa (UTS) with a microstructure characterized by fine and equiaxed grains under optimal conditions. In contrast, our research yielded a tensile strength of 317 MPa when utilizing the new tool design, with a differences of 125.38 MPa in comparison with [31], highlighting the superior performance of our tool design in enhancing the welding process and mechanical properties. Mumin Yilmaz et al. [47] studied FSW/P 1.1 mm thick DP600 steel sheets. The specimens were processed using a tungsten carbide (WC) tool with a pin diameter, pin length, and shoulder diameter of 14 mm, 5 mm, and 0.8 mm. The tool rotation axis was tilted by 3°, and the rotation speed and linear transition speed were set to 1000 rpm and 1.6 mm/s, respectively. Thermomechanical process conditions, such as plastic strain and temperature, resulted in the development of specific deformation regions, which are distinguished by their microstructural features. These deformation regions are referred to as the stir zone (SZ), thermo-mechanically affected zone (TMAZ), and heat-affected zone (HAZ) in accordance with previous research studies. It is important to note that the HAZ was narrow compared to the SZ and TMAZ. Friction stir processing strongly affected the as-received microstructure. We show for all samples the stir zone (SZ)/the weld nugget zone (WNZ) on the cross-section perpendicular to the tool transverse direction of the welded specimen with high tensile strength, composed of smaller and equiaxed grains. In the base metal, the grain size is not uniformed, elongated, or non-equiaxed, as shown in Figure 4.

The microstructure of SZ has very fine equiaxed dark crystal grains, while HAZ has larger equiaxed blue-white crystal grains, due to dynamic recrystallization during the FSW process.

Figure 6 provides a depiction of the intricate microstructures present within various sections of a dissimilar alloy (specifically, the transition from AA6061 to AA5083) FSW joint, utilizing a new tool design. This detailed examination reveals distinctive zones within the microstructure, each with its own unique characteristics and significance. The foremost region of interest in this analysis is the SZ, as depicted in Figure 6. This region constitutes the nugget zone, located precisely at the center of the weld. It is notable for being entirely recrystallized, signifying a transformation of the material in this vicinity during the welding process. The stir zone corresponds closely to the location where the newly designed tool pin engages with the materials during the welding operation. We observed a reduction in grain (Figure 6), with grains typically measuring an order of magnitude smaller than those found in normal materials. The stir zone, crucially, represents a harmonious amalgamation of both aluminum alloys, AA5083 and AA6061, displaying a seamless blending of these dissimilar materials.

Adjacent to the stir zone is the TMAZ, as portrayed in Figure 6a,b. Unlike the stir zone, the TMAZ is not subject to complete recrystallization. However, it bears the hallmark of being heavily influenced by the welding process's thermal and mechanical forces, which leads to substantial microstructural changes in this region. Moving further outward from the TMAZ, we encounter the HAZ, as illustrated in Figures 6a,c and 8. This particular zone experiences the effects of heat generated during welding but remains untouched by any significant plastic deformation. The HAZ represents a region where the microstructure has been primarily altered due to the thermal aspects of the welding process.

Finally, at the extremes of the cross-section, we find the BM regions. As seen in Figure 6b,f, the left side corresponds to AA5083, and the right side to AA6061. These regions remain largely unaffected by the welding process, serving as the pristine starting points for the dissimilar alloys. They are located a considerable distance away from the weld and thus remain structurally unaltered. Importantly, the observed microstructure aligns with findings from prior research conducted by other scholars [48]. This consistency reinforces the validity and reliability of the depicted microstructural zones within the dissimilar alloy FSW joint, thus contributing to our collective understanding of this complex welding process.

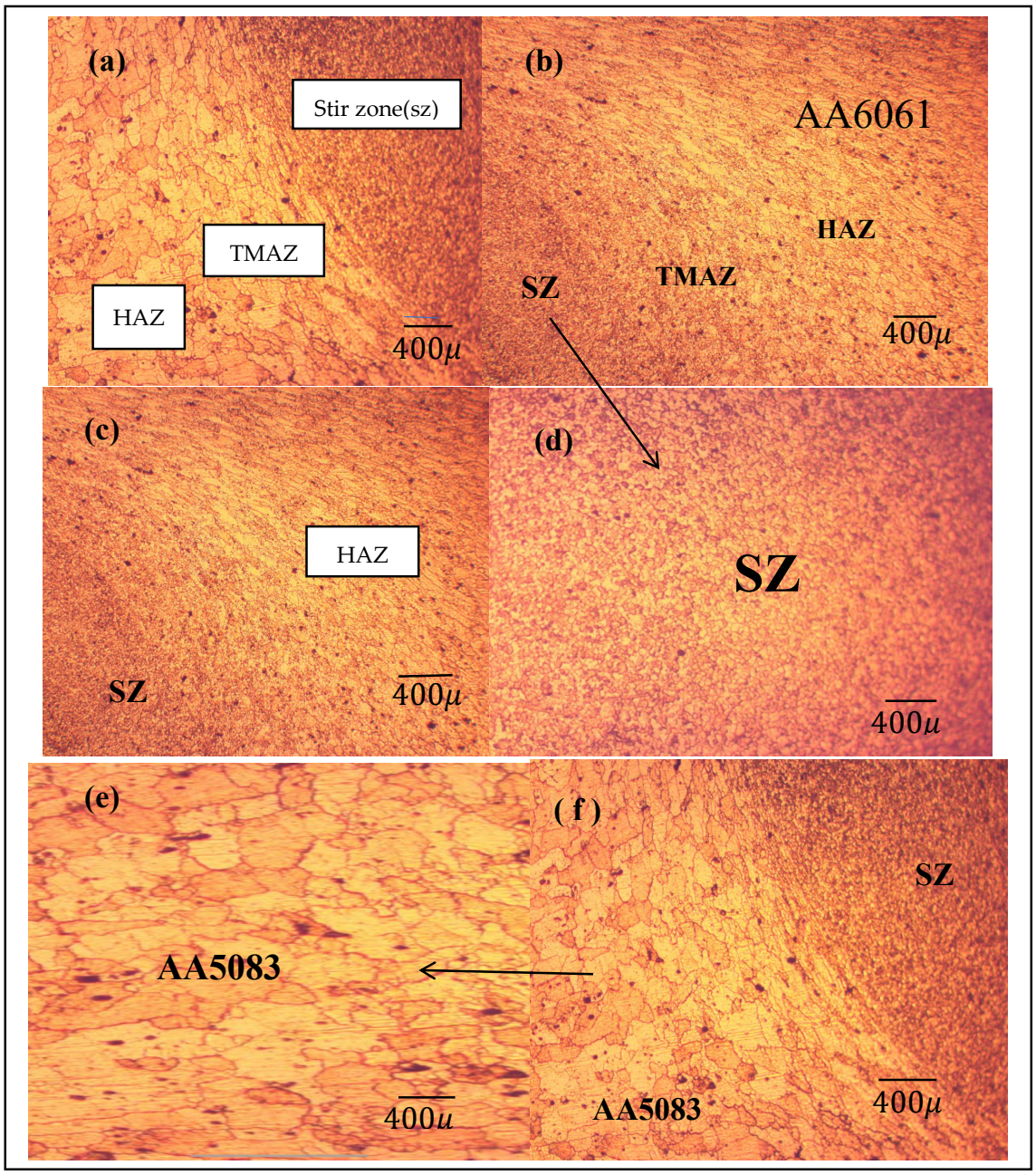

Figure 6. The microstructure of the welded joint. The microstructure of the optimum TS of FSW for the new tool design. (**a**) left-side base metal (BM) is AA5083, corresponding to the advancing side. (**b**) Adjacent to the advancing side is the thermo-mechanically affected zone (TMAZ). (**c**) Beyond the TMAZ lies the HAZ. (**d**) At the joint's center is the SZ, also known as the nugget zone. (**e**) On the retreating side, another TMAZ is observed. (**f**) The right-side BM consists of AA6061 and is located on the retreating side.

3.3. Microhardness Analysis

Table 9 presents the microhardness results obtained under optimal tensile strength (TS) conditions using the new tool design. These microhardness values, measured in region (SZ) and in HV (Vickers microhardness), exhibit a range between 105 and 122. This variation, in conjunction with optimal tensile strengths, highlights the multifaceted nature of the FSW process, where numerous factors interact to shape the outcomes. One noteworthy observation is the potential relationship between tensile strength and microhardness. Notably, the sample with the highest TS, reaching 317 MPa, showcases the highest microhardness value

of 122. This correlation could be attributed to the inherent welding process mechanisms where higher tensile strengths might correspond to denser grain structures.

Table 9. Microhardness of the optimum TS of FSW with the new tool design.

No. of Samples	Optimize TS	Microhardness (Average SZ)	Error Margins
	MPa	HV	
1	285	120	15
2	280	118	11
5	317	122	17
7	290	105	20
8	270	105	25
18	278	105	20

Analyzing the presented data reveals insights into the relationship between the tensile strength (TS) and microhardness (HV) of various samples, with the processing parameters playing a crucial role. Specifically, Sample 5, subjected to parameters such as Th 3 mm and SS 1600 rpm., stands out with the highest TS at 317 MPa, while Sample 8, despite its thicker profile (Th 5 mm), registers the lowest TS at 270 MPa. Interestingly, even though Samples 3 and 7 share almost identical parameters. The variation in spindle speed (SS) seemingly dictates the difference in their TSs, emphasizing the SS's influence on material strength. Similarly, the subtle contrasts in length (L) and SS for Samples 8 and 18 account for their varied TSs, while the tensile strengths of Samples 2 and 1, having differing holding times (Tt) and feed rates (Fr), are relatively close, indicating Tt's potential negligible impact within certain bounds.

Investigating microhardness, the data highlight that it does not always align directly with TS. For instance, while Sample 5 showcases superior TS and HV, Samples 7 and 8, despite distinct TS values, converge at an HV of 105. This divergence hints at the fact that while certain processing parameters distinctly influence TS, they might affect hardness differently, suggesting independent modulating factors for deformation resistance and pull resistance in a material.

Materials exhibit varied mechanical behaviors, with tensile strength (TS) measuring resistance to pulling forces and microhardness (HV) evaluating resistance to deformation (Figure 7). While both metrics indicate mechanical strength, they do not always correlate due to different testing mechanisms, material microstructures, and processing effects. For instance, hardness tests assess localized compressive stresses, while tensile tests gauge a material's response to elongated stresses. Moreover, a material's atomic or grain arrangement can affect its hardness and tensile strength differently. Thus, processing parameters that influence one property might not have the same impact on the other, emphasizing the need to understand these distinct modulating factors for precise material customization. The data obtained grant a preliminary understanding; a comprehensive exploration encompassing varied parameters is vital for decoding the intricate interplay between mechanical properties and processing conditions, paving the way for process optimization.

Table 9 and Figure 8 present the hardness values obtained from the analysis of the weld region and its adjacent areas, with a particular focus on the optimal sample, Sample 5, which exhibits an impressive hardness value of 317 MPa. This sample was created using the new tool design, elaborated in Figure 6, and its microstructure deserves attention.

The analysis reveals a substantial disparity between four distinct zones, each playing a pivotal role in the welding process. Firstly, the base metal (BM) region represents the original materials, with AA5083 on the left and AA6061 on the right, serving as the foundation for the welding process. Surrounding the weld, the TMAZ experiences significant thermal and mechanical influence, resulting in notable changes in its hardness properties. Similarly, on both sides of the weld, the HAZ reflects the impact of heat from the welding process, causing varying levels of hardness alteration. Lastly, the SZ, or block zone, embodies the

heart of the welding operation, where the two base metals are blended. The hardness characteristics of the SZ are particularly crucial, as they directly influence overall weld quality and structural integrity.

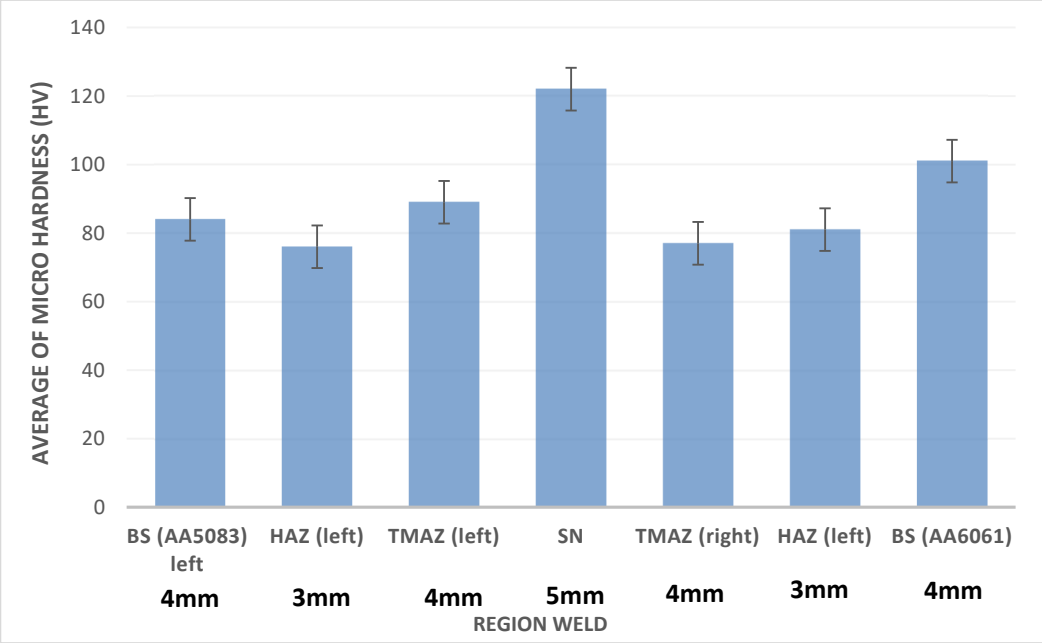

Figure 7. Average of microhardness (HV) in the region of weld Sample 5. Note: base metal (BM), heat-affected zone (HAZ), thermo-mechanically affected Zone (TMAZ). Error bars are for 95% confidence intervals.

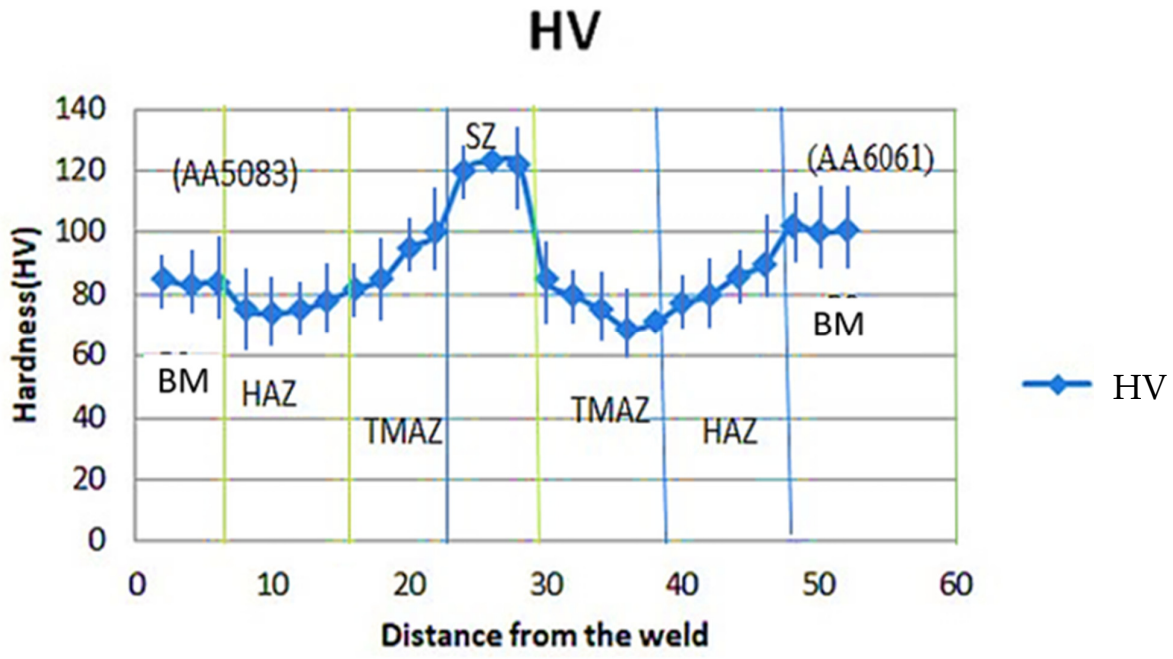

Figure 8. Microhardness profile of the FSW joint in Sample 3 (317 MPa) with the new tool design. Note: base metal (BM), heat-affected zone (HAZ), thermo-mechanically affected zone (TMAZ). Error bars are for 95% confidence intervals.

The variation in hardness values across these zones provides valuable insights into the effectiveness of the new tool design (Sample 5) and its impact on the resulting mi-

crostructure, as depicted in Figure 7. These findings highlight the importance of carefully considering and optimizing welding parameters and tool designs to achieve desired mechanical properties in welded structures.

The hardness observed at the center of the friction-stir-welded joint, specifically in the SZ, exhibits a greater value (with an average of 122 HV) compared to that in the HAZ. This hardness disparity in the nugget zone can be attributed to the phenomenon of recrystallization, which leads to the formation of a highly refined equiaxed grain structure. The HAZ regions exhibit a consistent decline in hardness, despite the nugget and flow arm zones displaying robust microstructure recovery owing to their very fine grain structure (Figure 6). In contrast, the TMAZ registers a slight upturn in hardness. Notably, the HAZ demonstrates a significant reduction in hardness values. This welding behavior aligns with prior research [1,10], but in our study, we observe higher hardness levels, indicating an enhancement resulting from the utilization of the new tool design. In a study conducted by [49], welding was performed using AA6061 with a 6 mm thickness, employing the standard FSW tool. Welding parameters included tool rotational speeds of 1400, 1200, and 1000 rpm., bed speeds of 30, 25, and 20 mm/min, and axial loads of 7, 6, and 5 KN. The resulting hardness values from various samples averaged 85, 77, and 87, respectively. Interestingly, when comparing these hardness values with those obtained using our new tool design, we observed higher hardness levels, despite the differences in alloy composition. In essence, FSW, with the new tool design, demonstrates its potential for strong and high-strength material joining through grain refinement mechanisms, further advancing our understanding of its applicability in advanced material applications. Eves Manuel et al. [50] welded FSW of three dissimilar aluminum alloys in a T-joint configuration. The base materials were the AA2017-T4, AA5083-H111, and AA6082-T6 alloys in 3 mm thick sheets. The tool had a (cylindrical and conical) threaded pin of 5.2 mm in length and a shoulder of 18 mm in diameter with a concavity of 5, and the tool's rotational speed (w-500 rpm), plunge depth (7.1 mm), and tilt angle (3) were maintained constant for all series. It appears that the increase in welding speed did not significantly change the hardness in the HAZ, either on the AA5083 or AA2017 sides. However, there was a slight decrease in hardness in the HAZ close to the tool path. The stir zone had an irregular hardness pattern with some peaks in the current welds as a result of the non-homogeneous mixing of the three different base materials during the process.

The HAZ softening is observed in Figure 8, which can be explained in conjunction with the microstructure in Figure 6. Based on Figure 8, HAZ softening may be caused by the complexity of material flow divergence between the weld metal, HAZ, and base metal. The HAZ is significant because it is a region where cracking may occur and because welding might lessen its characteristics in this region. Because HAZ's hardness is similar to that of the base metal, however, samples such as 1, 2, 5, 7, 8, and 18 exhibit neither observable cracking nor softening as grain growth was observed in BM, SZ, and TMAZ (Figure 6), which may be a result of strong heat transfer from the base metal to the area during the welding process.

Charpy V-Notch Test

Figure 9 displays the results of the Charpy impact test on the welded dissimilar aluminum alloys 6061-T6 and 5083-H111. This Figure provides an assessment of the samples' impact energy. The test results demonstrated that the new pin tool designs' impact strength was greater than that of normal tool designs in FSW. The 6061-T6 alloy sample created with the new pin tool design, in combination with the 5083-H111 material, exhibited superior impact resistance compared to the sample produced using the normal tool design. The innovative pin tool design, featuring both longitudinal and circular grooves, significantly enhances impact resistance and tensile strength in the welded material. These grooves act as barriers, preventing the dendrites from growing extensively and resulting in a finer, more compact structure. Moreover, they play a crucial role in improving the solidification process by controlling the cooling rates, ensuring a more uniform distribution of alloying elements,

and reducing the occurrence of defects within the material. These grooves contribute to stress redistribution during loading conditions, effectively lowering the risk of fractures.

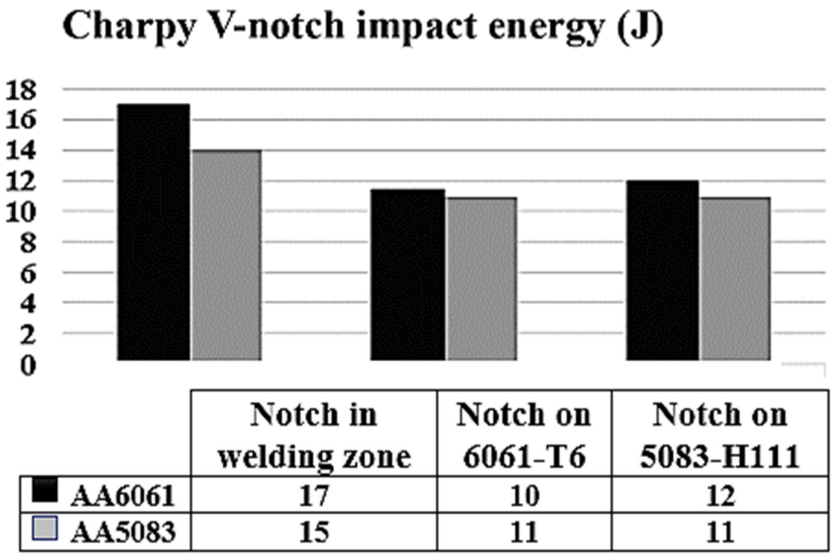

Figure 9. Results of the 6061-T6 with the 5083-H111 aluminum alloy using the Charpy V-notch test.

4. Conclusions

In comparative FSW tests involving normal and new tool designs, the new tool design exhibited a noteworthy increase in tensile strength, reaching 317 MPa. This represented an 18.2% improvement compared to the normal tool's tensile strength of 285 MPa. In addition, the joint efficiency saw a significant enhancement, rising from 83% to 92.2% with the new tool design. Utilizing RSM optimization, we identified the optimal parameters for achieving peak tensile strength for both tool designs. Several factors, such as holding time, aluminum thickness, pin length, feed rate, and spindle speed, were found to influence tensile strength. Notably, lower spindle speeds were preferable for achieving higher tensile strength. Microstructural analysis revealed that higher tensile strength was correlated with fewer microscopic defects (see Section 3.3). The hardness observed at the center of the friction-stir-welded joint, specifically in the SZ, exhibits a greater value (with an average of 122 HV) compared to that in the HAZ. This hardness disparity in the nugget zone can be attributed to the phenomenon of recrystallization, which leads to the formation of a highly refined equiaxed grain structure. Specifically, the microhardness of Sample 5 subjected to parameters of 3 mm thickness (Th), 25 s holding time (Tt), 0.1 mm dimension (L), 1600 rpm spindle speed (SS), and 30 mm/min feed velocity (Fr), exhibited the highest TS at 317 MPa. However, it is worth noting that the joint efficiency of the new tool design was slightly lower than that of the base alloy. Of particular significance is the superior impact resistance observed in samples created using the new pin tool design when paired with the 6061-T6 alloy and the 5083-H111 material. This contrasted with the samples produced using the normal tool design.

Author Contributions: Conceptualization: W.H.K., E.L.S. and M.R.B.I.; methodology, data collection and analysis, writing and drafting, literature review: W.H.K.; interpretation of results: W.H.K., E.L.S. and S.B.S.; overall supervision: E.L.S., M.R.B.I. and S.B.S. All authors have read and agreed to the published version of the manuscript.

Funding: This research received no external funding.

Data Availability Statement: The data presented in this study are available on request from the corresponding author due to the data that have been used are confidential.

Acknowledgments: The authors want to state that this study was conducted without external funding or financial support. The authors heartily thank the Department of Manufacturing Engineering, Universiti Tun Hussein Onn Malaysia (UTHM) for providing facilities for the research work. The authors are grateful to the Laboratory Manager at UTHM, Hamidon Bin Salleh, for providing testing facilities.

Conflicts of Interest: The authors declare no conflict of interest.

References

1. Jannet, S.; Mathews, K.; Raja, R. Comparative investigation of friction stir welding and fusion welding of 6061 T6—5083 O aluminum alloy based on mechanical properties and microstructure. *Bull. Polish Acad. Sci. Tech. Sci.* **2014**, *62*, 791–795. [CrossRef]
2. SGupta, K.; Pandey, K.N.; Kumar, R. Artificial intelligence-based modelling and multi-objective optimization of friction stir welding of dissimilar AA5083-O and AA6063-T6 aluminium alloys. *Proc. Inst. Mech. Eng. Part L J. Mater. Des. Appl.* **2018**, *232*, 333–342. [CrossRef]
3. Threadgilll, P.L.; Leonard, A.J.; Shercliff, H.R.; Withers, P.J. Friction stir welding of aluminium alloys. *Int. Mater. Rev.* **2009**, *54*, 49–93. [CrossRef]
4. Wang, B.B.; Xue, P.; Xiao, B.L.; Wang, W.G.; Liu, Y.D.; Ma, Z.Y. Achieving equal fatigue strength to base material in a friction stir welded 5083-H19 aluminium alloy joint. *Sci. Technol. Weld. Join.* **2020**, *25*, 81–88. [CrossRef]
5. Selvakumar, S.; Babu, B.G.; Raffic, N.M.; Babu, K.G. Experimental Investigation on Effect of FSW Parameters on Hardness and Microstructure of AA 6061 and AA 5083. 2020. Available online: https://www.ijresm.com/Vol.3_2020/Vol3_Iss2_February20/IJRESM_V3_I2_151.pdf (accessed on 12 February 2024).
6. Kumar, J.; Majumder, S.; Mondal, A.K.; Verma, R.K. Influence of rotation speed, transverse speed, and pin length during underwater friction stir welding (UW-FSW) on aluminum AA6063: A novel criterion for parametric control. *Int. J. Light. Mater. Manuf.* **2022**, *5*, 295–305. [CrossRef]
7. Kumar, K.S.; Seeman, M.; Sivaraj, P.; Balasubramanian, V. Mechanical properties and metallurgical characteristics of friction stir welded dissimilar AA5083/AA6061 aluminum alloy joints. In Proceedings of the IP Conference Proceedings, Boston, MA, USA, 21–22 September 2023; p. 2747. [CrossRef]
8. Mamgain, A.; Singh, V.; Singh, A.P. Influence of Welding parameters on Mechanical property during Friction Stir Welded joint on Aluminium Alloys: A Review. *J. Kejuruter* **2023**, *35*, 13–28. [CrossRef] [PubMed]
9. Gupta, M.K. Effects of tool profile on mechanical properties of aluminium alloy Al 1120 friction stir welds. *J. Adhes. Sci. Technol.* **2020**, *34*, 2000–2010. [CrossRef]
10. Rajaseelan, S.L.; Kumarasamy, S. Mechanical properties and microstructural characterization of dissimilar friction stir welded AA5083 and AA6061 aluminium alloys. *Mechanika* **2020**, *26*, 545–552. [CrossRef]
11. Elatharasan, G.; Manikandan, R.; Karthikeyan, G. Multi-response optimization of process parameters in friction stir welding of dissimilar aluminum alloys by Grey relation analysis (AA 6061-T6 & AA5083-H111). *Mater. Today Proc.* **2020**, *37*, 1172–1182. [CrossRef]
12. Lakshmikhanth, R.S.; Subbaiah, K. Optimization of Tool Pin Profile for Dissimilar Friction stir welding of AA5083-H111 and AA6061-T6 aluminum alloys. *Tierarztl. Prax.* **2020**, *40*, 460–473.
13. Kumar, K.K.; Kumar, A.; Satyanarayana, M.V.N.V. Effect of friction stir welding parameters on the material flow, mechanical properties and corrosion behavior of dissimilar AA5083-AA6061 joints. *Proc. Inst. Mech. Eng. Part C J. Mech. Eng. Sci.* **2022**, *236*, 2901–2917. [CrossRef]
14. Tucci, F.; Carlone, P.; Silvestri, A.T.; Parmar, H.; Astarita, A. Dissimilar friction stir lap welding of AA2198-AA6082: Process analysis and joint characterization. *CIRP J. Manuf. Sci. Technol.* **2021**, *35*, 753–764. [CrossRef]
15. Astarita, A.; Tucci, F.; Silvestri, A.T.; Perrella, M.; Boccarusso, L.; Carlone, P. Dissimilar friction stir lap welding of AA2198 and AA7075 sheets: Forces, microstructure and mechanical properties. *Int. J. Adv. Manuf. Technol.* **2021**, *117*, 1045–1059. [CrossRef]
16. Reimann, M.; Goebel, J.; Santos, J.F.D. Microstructure and mechanical properties of keyhole repair welds in AA 7075-T651 using refill friction stir spot welding. *Mater. Des.* **2017**, *132*, 283–294. [CrossRef]
17. Palanivel, R.; Mathews, P.K.; Murugan, N.; Dinaharan, I. Effect of tool rotational speed and pin profile on microstructure and tensile strength of dissimilar friction stir welded AA5083-H111 and AA6351-T6 aluminum alloys. *Mater. Des.* **2012**, *40*, 7–16. [CrossRef]
18. Pereira, M.A.R.; Galvão, I.; Costa, J.D.; Leal, R.M.; Amaro, A.M. Friction Stir Spot Welding of Thin Aluminium Sheets to Polyamide 6: A Study of the Welding Parameters and Strategies. *J. Compos. Sci.* **2024**, *8*, 21. [CrossRef]
19. Ahmadi, M.; Pahlavani, M.; Rahmatabadi, D.; Marzbanrad, J.; Hashemi, R.; Afkar, A. An Exhaustive Evaluation of Fracture Toughness, Microstructure, and Mechanical Characteristics of Friction Stir Welded Al6061 Alloy and Parameter Model Fitting Using Response Surface Methodology. *J. Mater. Eng. Perform.* **2022**, *31*, 3418–3436. [CrossRef]
20. Kumar, P.S.; Chander, M.S. Effect of tool pin geometry on FSW dissimilar aluminum alloys—(AA5083 & AA6061). *Mater. Today Proc.* **2020**, *39*, 472–477. [CrossRef]
21. Verma, S.; Kumar, V. Optimization of friction stir welding parameters of dissimilar aluminium alloys 6061 and 5083 by using response surface methodology. *Proc. Inst. Mech. Eng. Part C J. Mech. Eng. Sci.* **2021**, *235*, 7009–7020. [CrossRef]

22. Khodir, S.A.; Shibayanagi, T. Friction stir welding of dissimilar AA2024 and AA7075 aluminum alloys. *Mater. Sci. Eng. B Solid-State Mater. Adv. Technol.* **2008**, *148*, 82–87. [CrossRef]
23. Cavaliere, P.; De Santis, A.; Panella, F.; Squillace, A. Effect of welding parameters on mechanical and microstructural properties of dissimilar AA6082-AA2024 joints produced by friction stir welding. *Mater. Des.* **2009**, *30*, 609–616. [CrossRef]
24. Zhang, T.; Ji, H.; Xu, D.; Yin, X.; Wei, H.; Sun, Z.; Liu, C. A hybrid shoulder to achieve a significant improvement in tensile strength and fatigue performance of friction stir welded joints for Al–Mg–Si alloy. *J. Mater. Res. Technol.* **2023**, *27*, 2280–2291. [CrossRef]
25. Homola, P.; Růžek, R.; McAndrew, A.R.; De Backer, J. Effect of primer and sealant in refill friction stir spot welded joints on strength and fatigue behaviour of aluminium alloys. *Int. J. Fatigue* **2023**, *168*, 107455. [CrossRef]
26. Hassan, K.S.; Abbass, M.K.; Mohammed, M.T. Effect of Surface Finishing on Microstructure and Corrosion Behavior of Friction Stir Welded Joints For Dissimilar Aluminum Alloys (AA2024-T3 with AA6061-T6). *IOP Conf. Ser. Mater. Sci. Eng.* **2021**, *1105*, 012047. [CrossRef]
27. Li, X.; Fang, J.; Guan, X. Unified Principal S–N Equation for Friction Stir Welding of 5083 and 6061 Aluminum Alloys. *Chin. J. Mech. Eng.* **2021**, *34*, 15. [CrossRef]
28. Shaik, C.B.; Pawale, D.M.; Suryanarayanan, R.; Sridhar, V.G. Improving the Mechanical properties of 6061 and 5083 welded joint using Friction stir lap welding. *J. Phys. Conf. Ser.* **2021**, *1969*, 012017. [CrossRef]
29. Pereira, M.A.R.; Galv, I.; Costa, D.; Amaro, A.M. Joining of Fibre-Reinforced Thermoplastic Polymer Composites by Friction Stir Welding—A Review. *Appl. Sci.* **2022**, *12*, 2744. [CrossRef]
30. Sidhu, M.S.; Chatha, S.S. Friction Stir Welding—Process and its Variables: A Review. *Int. J. Emerg. Technol. Adv. Eng.* **2012**, *2*, 275–279.
31. Jayaprakash, S.; Siva Chandran, S.; Sathish, T.; Gugulothu, B.; Ramesh, R.; Sudhakar, M.; Subbiah, R. Effect of tool profile influence in dissimilar friction stir welding of aluminium alloys (AA5083 and AA7068). *Adv. Mater. Sci. Eng.* **2021**, *2021*, 7387296. [CrossRef]
32. Testing, P. Effect of tool material on microstructure and mechanical properties in friction stir welding. *Mater. Test.* **2016**, *58*, 36–42.
33. Organized, T.; Degree, A.M.; Energy, R. Effect of Holding Time on the Physical Mechanical Properties of Dissimilar Metal Diffusion Welded between Aluminum and Steel by Ali Jebril Saad Jebril Nim: S951208008 Postgraduate Program. Ph.D. Thesis, UNS (Sebelas Maret University), Kota Surakarta, Indonesia, 2014.
34. Piccini, J.M.; Svoboda, H.G. Effect of pin length on Friction Stir Spot Welding (FSSW) of dissimilar Aluminum-steel joints. *Procedia Mater. Sci.* **2015**, *9*, 504–513. [CrossRef]
35. Wronska, A.; Andres, J.; Altamer, T.; Dudek, A.; Ulewicz, R. Effect of tool pin length on microstructure and mechanical strength of the FSW joints of Al 7075 metal sheets. *Commun. Sci. Lett. Univ. Žilina* **2019**, *21*, 40–47. [CrossRef]
36. Ahmed, M.M.Z.; Seleman, M.M.E.S.; Eid, R.G.; Albaijan, I.; Touileb, K. The Influence of Tool Pin Geometry and Speed on the Mechanical Properties of the Bobbin Tool Friction Stir Processed AA1050. *Materials* **2022**, *15*, 4684. [CrossRef] [PubMed]
37. El Rayes, M.M.; Soliman, M.S.; Abbas, A.T.; Pimenov, D.Y.; Erdakov, I.N.; Abdel-Mawla, M.M. Effect of Feed Rate in FSW on the Mechanical and Microstructural Properties of AA5754 Joints. *Adv. Mater. Sci. Eng.* **2019**, *2019*, 4156176. [CrossRef]
38. Hunt, F.; Badarinarayan, H.; Okamoto, K. *Design of Experiments for Friction Stir Stitch Welding of Aluminum Alloy 6022-T4—Friction Stir Welding of Aluminum for Automotive Applications (3)*; SAE Technical Paper 2006-01-0970; SAE International: Warrendale, PA, USA, 2006. [CrossRef]
39. Khanna, N.; Bharati, M.; Sharma, P.; Badheka, V.J. Design-of-experiments application in the friction stir welding of aluminium alloy AA 8011-h14 for structural application. *Multidiscip. Model. Mater. Struct.* **2020**, *16*, 606–622. [CrossRef]
40. Kumar, K.K.; Kumar, A.; Satyanarayana, M.V.N.V. Enhancing corrosion resistance and mechanical properties of dissimilar friction stir welded 5083-6061 aluminium alloys using external cooling environment. *Proc. Inst. Mech. Eng. Part L J. Mater. Des. Appl.* **2021**, *235*, 2692–2708. [CrossRef]
41. Kumar, S.; Gupta, E.D. Optimization of Submerged Arc Welding Parameters for Joining Dissimilar Materials Using Taguchi Method. *IOSR J. Mech. Civ. Eng.* **2017**, *14*, 51–54. [CrossRef]
42. Mustafa, F.F.; Kadhym, A.H.; Yahya, H.H. Tool geometries optimization for friction stir welding of AA6061-T6 aluminum alloy T-joint using taguchi method to improve the mechanical behavior. *J. Manuf. Sci. Eng. Trans. ASME* **2015**, *137*, 031018. [CrossRef]
43. Rajak, D.K.; Pagar, D.D.; Menezes, P.L.; Eyvazian, A. Friction-based welding processes: Friction welding and friction stir welding. *J. Adhes. Sci. Technol.* **2020**, *34*, 2613–2637. [CrossRef]
44. Rahmatabadi, D.; Shahmirzaloo, A.; Hashemi, R.; Farahani, M. Using digital image correlation for characterizing the elastic and plastic parameters of ultrafine-grained Al 1050 strips fabricated via accumulative roll bonding process. *Mater. Res. Express* **2019**, *6*, 086542. [CrossRef]
45. Sharma, A.; Dwivedi, V.K.; Singh, Y.P. Effect on ultimate tensile strength on varying rotational speed, plunge depth and welding speed during friction stir welding process of aluminium alloy AA7075. *Mater. Today Proc.* **2019**, *26*, 2055–2057. [CrossRef]
46. Ramesh, N.R.; Kumar, V.S.S. Experimental erosion-corrosion analysis of friction stir welding of AA 5083 and AA 6061 for sub-sea applications. *Appl. Ocean Res.* **2020**, *98*, 102121. [CrossRef]
47. Yilmaz, M.; Yilmaz, I.O.; Saray, O. Fatigue and Impact Behavior of Friction Stir Processed Dual-Phase (DP600) Steel Sheets. *Metals* **2024**, *14*, 305. [CrossRef]

48. Zainulabdeen, A.A.; Abbass, M.K.; Ataiwi, A.H.; Khanna, S.K.; Jashti, B.; Widener, C. Investigation of Fatigue Behavior and Fractography of Dissimilar Friction Stir Welded Joints of Aluminum Alloys 7075-T6 and 5052-H34. *Int. J. Mater. Sci. Eng.* **2014**, *2*, 115–121. [CrossRef]
49. Asmare, A.; Al-Sabur, R.; Messele, E. Experimental investigation of friction stir welding on 6061-t6 aluminum alloy using taguchi-based gra. *Metals* **2020**, *10*, 1480. [CrossRef]
50. Manuel, N.; Galvão, I.; Leal, R.M.; Costa, J.D.; Loureiro, A. Nugget formation and mechanical behaviour of friction stirwelds of three dissimilar aluminum alloys. *Materials* **2020**, *13*, 2664. [CrossRef]